LETTER

Point-defect management in homoepitaxially grown Si-doped GaN by MOCVD for vertical power devices

Applied Physics Express 15, 051003 (2022)
https://doi.org/10.35848/1882-0786/ac6566

LETTER

Point-defect management in homoepitaxially grown Si-doped GaN by MOCVD for vertical power devices

Shashwat Rathkanthiwar[1*], Pegah Bagheri[1], Dolar Khachariya[2], Seiji Mita[3], Spyridon Pavlidis[2], Pramod Reddy[3], Ronny Kirste[3], James Tweedie[3], Zlatko Sitar[1,3], and Ramón Collazo[1]

[1]Department of Materials Science and Engineering, North Carolina State University, Raleigh, North Carolina 27695-7919, United States of America
[2]Department of Electrical and Computer Engineering, North Carolina State University, Raleigh, North Carolina 27695-7911, United States of America
[3]Adroit Materials, Inc., 2054 Kildaire Farm Rd., Cary, North Carolina 27518, United States of America

*E-mail: srathka@ncsu.edu

Received March 31, 2022; revised April 4, 2022; accepted April 6, 2022; published online April 14, 2022

We demonstrate controlled Si doping in the low doping range of 5×10^{15}–2.5×10^{16} cm^{-3} with mobility >1000 cm^2 V^{-1} s^{-1} in GaN films grown by metalorganic chemical vapor deposition. The carbon-related compensation and mobility collapse were prevented by controlling the electrochemical potential near the growth surface via chemical potential control (CPC) and defect quasi-Fermi level (dQFL) point-defect management techniques. While the CPC was targeted to reduce the net C_N concentration, the dQFL control was used to reduce the fraction of C atoms with the compensating configuration, i.e. C_N^{-1}. The low compensating acceptor concentration was confirmed via temperature-dependent Hall effect analysis and capacitance–voltage measurements. © 2022 The Japan Society of Applied Physics

The demand for next-generation, kV-class power electronics is increasing for applications in electric motor drives, energy storage, power conversion, and energy distribution.[1–3] Gallium nitride (GaN)-based vertical diodes and switches are poised to enable highly-efficient power devices, thanks to their wide bandgap and low on-resistance, correlating to a Baliga's figure of merit that is several orders of magnitude higher than that of Si and three times higher than that of SiC.[4,5] The development of thick n-GaN drift layers with controllable doping in the range of 10^{15}–10^{16} cm^{-3} is the key to the realization of kV-class, GaN-based power devices.[6] Although quasi-vertical devices based on heteroepitaxially-grown GaN epilayers on SiC, sapphire, and Si (111)[4,5,7] have been demonstrated for <1 kV breakdown voltage, these epi-stacks exhibit high threading dislocation densities, exceeding 10^8 cm^{-2}, thereby, deleteriously impacting the device lifetime and performance both in the ON and OFF states. While the screw dislocations enhance the reverse leakage,[8] threading edge dislocations induce electron traps, at about every c-lattice translation.[9] For instance, a threading edge dislocation density of 5×10^8 cm^{-2} correlates to a trap concentration of $\sim 10^{16}$ cm^{-3}. These traps not only compensate the free electrons in the drift layers but also lead to significantly reduced electron mobilities, rendering heteroepitaxially-grown GaN films unsuitable for kV-class, vertical power devices.[10] The commercialization of single-crystal GaN substrates by the ammonothermal method has enabled the homoepitaxial growth of low dislocation density ($<10^5$ cm^{-2}) GaN epilayers.[11,12] This has propelled the development of kV-class, vertical power devices based on high-mobility, lightly-doped GaN drift layers with reliable doping in the doping range $<2 \times 10^{16}$ cm^{-3}.

Although metalorganic chemical vapor deposition (MOCVD) remains the commercially-preferred technique that enables excellent control over doping, there have been few MOCVD reports on controlled low n-doping ($<10^{16}$ cm^{-3}) with high electron mobility.[11,13] While the homoepitaxial growth of GaN minimizes the formation of threading dislocations and associated traps, the incorporation of compensating background impurities, especially carbon (C_N), during the MOCVD growth has presented a major challenge to achieving controllable doping in the low doping range.[13–15] The most commonly employed approach for controling carbon incorporation in GaN epilayers is by controlling its chemical potential that can be accessed via various MOCVD growth parameters. In addition to carbon, iron (Fe_{Ga}) has been observed to constitute as a compensation center.[16–19] While it is generally accepted that the metalorganic precursor is the primary source of carbon, the source of iron was traced to stainless-steel parts,[19] sub-percentage level iron impurities in the graphite susceptors typically used in radio frequency heating systems[17,18] and to contamination during wafer cleaning.[18] There have been multiple reports targeting the reduction of both C_N and Fe_{Ga} defects,[10,16–18,20] however, carbon-related compensation remains the primary bottleneck in the realization of controllable low doping in MOCVD.[11,13,14]

All samples in this study were grown in a vertical, cold-walled, low-pressure, RF-heated MOCVD reactor at a growth temperature of 1300 K and total pressure of 20 Torr. Figures 1(a) and 1(b) show the respective epi-stacks for the two sets of samples grown on *c*-plane sapphire and semi-insulating, *c*-plane, ammonothermal GaN substrates (Ammono, SA) with a miscut of 0.4° towards the *m*-plane. The surface preparation of GaN substrates involved sequential 1 min steps of 10% HF solution, DI water, 10% HCl solution and isopropanol. Samples grown on sapphire incorporated a 250 nm thick, high-temperature AlN layer to reduce dislocation density in n-GaN epilayers to $\sim 1 \times 10^9$ cm^{-2}. Prior to n-GaN growth, 1 μm thick, high-resistivity (HR) GaN epilayer with 5×10^{18} cm^{-3} carbon was grown on both substrates for electrical isolation and served at the same time as a diffusion barrier for possible impurities from the substrate. The top n-GaN layers were 1 μm thick and doped with Si in the range between 0.7–3 $\times 10^{16}$ cm^{-3}. The carbon concentration in these layers was targeted to be a few times lower than that of the Si dopant and was maintained either at $\sim 9 \times 10^{15}$ cm^{-3} or $\sim 3 \times 10^{15}$ cm^{-3} by controling chemical potential[10,20] via organometallic flow, corresponding to V/III ratios of 4000 and 8000, respectively. A similar carbon concentration was measured on sapphire and GaN substrates by secondary ion mass spectroscopy (SIMS) conducted at Evans Analytical Group using the low C measurement protocol. In order to further reduce compensation, the

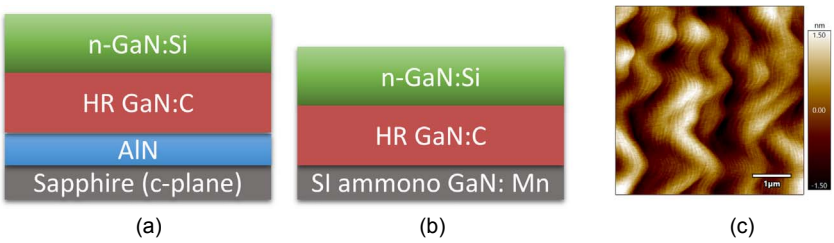

Fig. 1. (Color online) (a) and (b) show the epi-stacks for the growth of Si-doped GaN on sapphire and Mn-doped semi-insulating native GaN substrates, respectively (c) shows the surface morphology of the homoepitaxially grown GaN epilayer.

fraction of carbon atoms in the acceptor state was managed via defect quasi-Fermi level (dQFL) control that was previously demonstrated for Si doping levels $>5 \times 10^{17}$ cm^{-3}.[21–23] In this process, the minority carriers required to control the Fermi level (E_F) were generated via above-bandgap illumination (Hg-Xe lamp) at a power density of 1 W cm^{-2}. Figure 2 shows the enhancement in the formation energy of the C acceptor (C_N^{-1}) as a function of E_F under ultraviolet illumination.[21]

The threading edge dislocation density (ρ^{edge}) in the epi-stacks grown on sapphire was determined by performing (302) X-ray rocking curve measurements in a Philips X'Pert materials research diffractometer with a 4-bounce monochromator in a double-axis configuration. The N_A related to edge dislocations was estimated using the equation $N_A^{edge} = f \cdot (\rho^{edge}/c)$, where f is the fraction of trap occupancy at every c-lattice translation along the edge dislocation core, considered to be 0.5,[9] and c is the (0001) lattice parameter of the wurtzite GaN crystal. The surface morphology of the homoepitaxially grown GaN epilayer [Fig. 1(c)] was acquired in a tapping mode using Asylum Research MFP-3D atomic force microscope (AFM). Carrier concentration and mobility were measured in the range of 80–300 K using an 8400 series LakeShore AC/DC Hall measurement system. The Hall structures were prepared by e-beam evaporation of V/Al/Ni/Au metal stacks at the corners of 1×1 cm^2 samples in a van der Pauw geometry. Contact annealing was performed at 1120 K in N_2 ambient for 30 s. After Hall measurements, Ni/Au Schottky contacts were deposited for capacitance–voltage (CV) measurements to determine N_D–N_A.

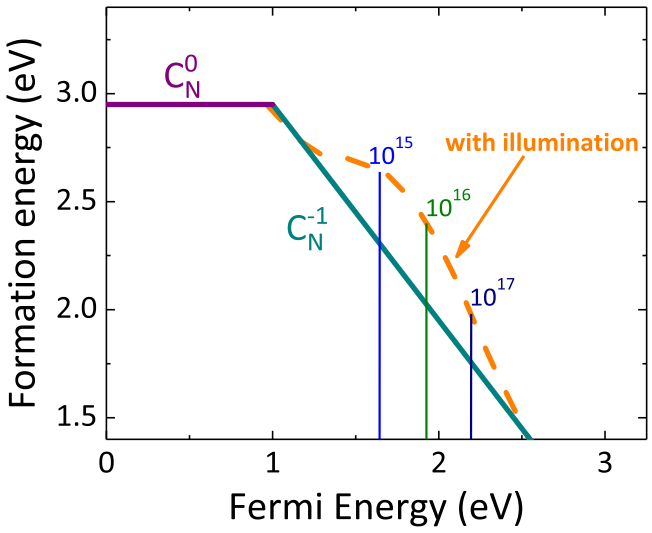

Fig. 2. (Color online) The formation energy of C_N in GaN at equilibrium (solid line) and under UV illumination (dashed line). A large increase in the formation energy of C_N^{-1} is estimated for the low doping range of 10^{15}–10^{16} cm^{-3} under ultraviolet illumination. Note. The vertical lines correspond to three different Si doping levels: 10^{15}, 10^{16} and 10^{17} cm^{-3} and were calculated for the growth temperature (1300 K) using semiconductor statistics and charge neutrality.

Table I shows the electron concentration and mobility values in n-GaN measured using Hall effect measurements. A large difference between Si (N_D) and electron (n) concentrations, indicative of significant compensation, can be observed for all samples grown on sapphire. This is expected because of the cumulative compensation owing to edge dislocations and carbon. The dislocation-induced trap density (N_A^{edge}) was estimated at $\sim 1 \times 10^{16}$ cm^{-3} based on the measured edge dislocation density of $\sim 1 \times 10^9$ cm^{-2}. A similar compensation effect was assigned to the 0.9×10^{16} cm^{-3} concentration of carbon, assuming that all the carbon atoms are incorporated in a compensating (acceptor) configuration, i.e. C_N^{-1}.[21] Thus, total compensator concentration (N_A) related to carbon and edge dislocations was estimated to be $\sim 2 \times 10^{16}$ cm^{-3}. The measured free electron concentration showed a good match with the N_D–N_A value. Also, the expected mobility collapse[10] was observed for Si concentrations approaching the total N_A value, with the mobility dropping to only 75 cm^2 V^{-1} s^{-1} for the lowest Si doping.

To examine the efficacy of the dQFL control approach in this relatively low doping range, similarly-doped samples were grown on sapphire under external UV illumination. Drastic improvements in mobility and electron concentration were observed for both Si concentrations (Table I), showing a net increase in free electron concentration of $\sim 7 \times 10^{15}$ cm^{-3}. This can be correlated to a net reduction in the concentration of carbon in the compensating (acceptor), C_N^{-1} configuration to $\sim 2 \times 10^{15}$ cm^{-3}, which is consistent with the expected formation energy and defect concentration changes from Fig. 2. It is noted that the UV illumination does not change the net carbon concentration in the n-GaN layer suggesting that a majority fraction of carbon atoms likely get incorporated in a non-compensating configuration.[23]

The estimated magnitude of dislocation-related compensation was verified by growing a similar set of samples on single crystalline GaN substrates with dislocation density $<10^5$ cm^{-2}. For a nominal Si doping of 2.5×0^{16} cm^{-3}, a clear increase in both free electron concentration and mobility was observed, as seen in Table I. The net increase in the free electron concentration by $\sim 1 \times 10^{16}$ cm^{-3} correlated well with the dislocation-induced trap density estimated for sapphire-based samples confirming the negligible contribution of dislocations in samples grown on GaN. The reduced

Table I. Nominal silicon concentration (N_d), use of above-bandgap excitation (UV illum.), carbon concentration (C), trap concentration induced by edge dislocations (N_A^{edge}), Hall carrier concentration (n), and Hall mobility (μ) for different samples in this study grown on sapphire and GaN substrates.

Substrate	Si (N_D) $\times 10^{16}$(cm^{-3})	UV	$C \times 10^{16}$(cm^{-3})	$N_A^{edge} \times 10^{16}$($cm^{-3}$)	$n \times 10^{16}$(cm^{-3})	μ (cm^2 V^{-1} s^{-1})
Sapphire	3	No	0.9	~1	0.5	210
	2.5	No	0.9	~1	0.3	75
	3	Yes	0.9	~1	1.2	650
	2.5	Yes	0.9	~1	0.95	620
GaN	2.5	Yes	0.9	<0.01	1.9	960
	1.3	Yes	0.3	<0.01	0.9	1020
	0.7	Yes	0.3	<0.01	0.5	1050

compensation leads to an enhancement in mobility due to reduced ionized impurity scattering.

The next sample was designed for a lower nominal doping level of 1.3×10^{16} cm^{-3}. To reduce the [C_N^{-1}]-related compensation, a higher V/III ratio of 8000 was used to reduce carbon incorporation to $\sim 3 \times 10^{15}$ cm^{-3}. For understanding the other sources of compensation in samples grown on GaN, temperature-dependent carrier concentration measurements were performed using Hall effect measurements in the temperature range of 80–300 K, as shown in Fig. 3(a). The conductive film thickness for Hall effect analysis was determined by accounting for the depletion layer widths at the surface and at the interface with the underlying C-doped GaN layer.[11] The depletion widths are evident in the C–V plot shown in Fig. 3(b). The solid curve in Fig. 3(a) represents the best fit using charge balance equations and semiconductor statistics[11] with fitting parameters N_D and N_A, and a donor ionization energy, E_{Si} of 30 meV.[24] Expectedly, the extracted N_D values for the two samples were found to be in good agreement with the nominal Si doping concentration. A similar N_A/N_D ratio of 0.32 was extracted for both samples, corresponding to an N_A of 8×10^{15} and 4×10^{15} cm^{-3}, respectively. As shown in Fig. 3(b), C–V measurements revealed effective donor concentrations (N_D–N_A) of $\sim 2 \times 10^{16}$ cm^{-3} and $\sim 1 \times 10^{16}$ cm^{-3} for the two samples, in good agreement with the value extracted from the fitting of the Hall measurement data. Next, the temperature-dependency of the Hall mobility was estimated using Matthiessen's rule for the dominant scattering mechanisms including polar optical phonon scattering, acoustic deformation potential scattering, piezoelectric scattering, neutral impurity scattering, dislocation scattering, and ionized impurity scattering.[9,11,13] As shown in Fig. 3(c), the theoretically estimated mobility showed a reasonable agreement with the experimental data for the two samples. For the sample grown with lower Si (1.3×10^{16} cm^{-3}) doping, the reduced N_A and N_D values both correlate to a decrease in the ionized impurity scattering, as is evident at lower temperatures.[11] The peak mobility value at low temperatures is a characteristic of the degree of compensation in n-GaN with a higher value implying lower compensation. The peak mobility measured 3980 cm^2 V^{-1} s^{-1} at 110 K which is an improvement over the highest reported values for lightly-doped n-GaN grown by molecular beam epitaxy (3327 cm^2 V^{-1} s^{-1})[9] and sputtering (3470 cm^2 V^{-1} s^{-1})[25] but is lower than the highest reported values for MOCVD (6660 cm^2 V^{-1} s^{-1})[13] and hydride vapor phase epitaxy (7386 cm^2 V^{-1} s^{-1}).[26]

Coming back to the discussion on compensation in these samples, interestingly, the N_A values of 8×10^{15} cm^{-3} and 4×10^{15} cm^{-3} are about the same as the carbon concentrations. However, following the observations on samples grown on sapphire, the dQFL control is expected to reduce the [C_N^{-1}] by >3-fold of the net carbon concentration, to $<3 \times 10^{15}$ cm^{-3} and $<1 \times 10^{15}$ cm^{-3}, respectively, in these two samples. This suggests the presence of compensating defects other than carbon at the $\sim 10^{15}$ cm^{-3} level. These may include impurity defects such as Fe_{Ga} or Mn_{Ga},[27] as observed before[14,16–18] or intrinsic defects such as V_{Ga}-related defects.[28] While the V_{Ga}-related defects could result due to the use of a low gallium chemical potential (high V/III ratio), the Fe might originate from the stainless-steel parts, SiC coated graphite susceptor or wafer cleaning induced contamination.[16–19] Also, as was shown recently, despite the use of a buffer layer, Mn diffusion tail from the Mn-doped GaN substrate could be present at the $\sim 10^{15}$ cm^{-3} level.[14] It is to be noted that while the dQFL control is expected to reduce all compensating defects,[21,23] as to how efficiently the dQFL suppresses the compensation due to Fe, Mn, gallium vacancies and dislocation-related deep traps would depend on the ionization energy and charge state of

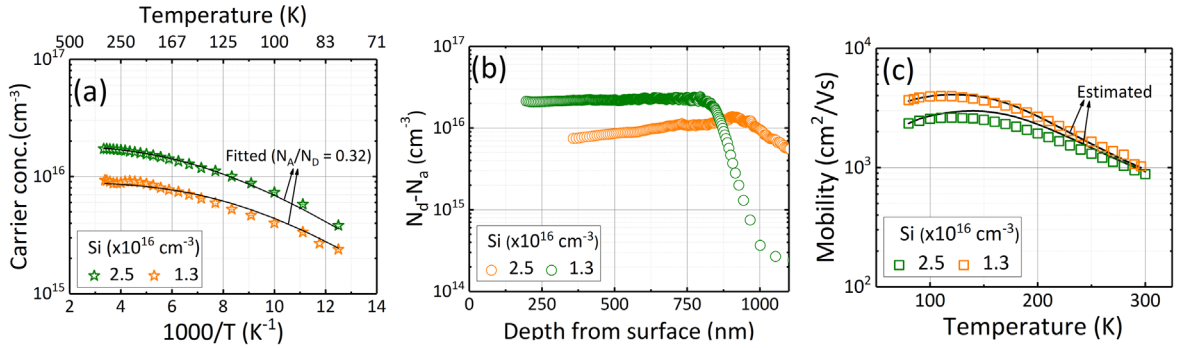

Fig. 3. (a) Temperature dependence of the carrier concentration (b) depth dependence of the effective donor concentration (c) temperature dependence of the experimentally measured and theoretically estimated mobility values for samples grown on GaN substrate with 2.5×10^{16} and 1.3×10^{16} cm^{-3} Si concentration. The physical constants used for the estimation of theoretical mobility were based on Ref. 9.

the defects. Finally, for the sample with the lowest N_D value in this study, the room temperature carrier concentration and mobility measured 5×10^{15} cm^{-3} and 1050 cm^2 V^{-1} s^{-1}, respectively (Table I). This is one of the lowest doping values realized by MOCVD while maintaining high mobility.

In conclusion, this study demonstrates the consummate promise of systematic point-defect management during crystal growth of n-GaN epilayers to reliably achieve low carrier concentrations in the range of 10^{15} cm^{-3}, which is required for the development of kV-class GaN-based vertical power devices. The high efficacy of the dQFL control approach in the low doping range of $\sim 10^{16}$ cm^{-3} was confirmed on Si-doped GaN epilayers grown on sapphire substrates where a >3-fold reduction in $[C_N^{-1}]$ from 9×10^{16} cm^{-3} to $<3 \times 10^{15}$ cm^{-3} was observed. With controlled Si doping at 2.5×10^{16} cm^{-3}, the reduction in $[C_N^{-1}]$ resulted in the mobility and carrier concentration increase from 60 to 620 cm^2 V^{-1} s^{-1} and 3×10^{15} to 10^{16} cm^{-3}, respectively. Si-doped GaN grown on GaN substrates with a synergistic combination of chemical potential control and dQFL control to reduce compensation showed controllable and reliable doping with carrier concentrations in the range of 5×10^{15}–2×10^{16} cm^{-3} with room temperature mobility exceeding 1000 cm^2 V^{-1} s^{-1}. This study demonstrates the utility of dQFL control in ensuring low carbon-related compensation while retaining high growth rates, which is of critical importance for growing thick drift layers using MOCVD. This work is, therefore, expected to pave the way towards the needed defect engineering technology in wide bandgap semiconductors for kV-class power electronics.

Acknowledgments The authors acknowledge funding in part from AFOSR (FA9550-17-1-0225, FA9550-19-1-0114, FA9550-19-1-0358), NSF (ECCS-1508854, ECCS-1916800, ECCS-1653383), and ARO (W911NF-16-C-0101).

ORCID iDs Shashwat Rathkanthiwar https://orcid.org/0000-0003-0180-1398 Dolar Khachariya https://orcid.org/0000-0002-8780-4583

1) H Amano et al., J. Phys. D **51**, 163001 (2018).
2) J. Y. Tsao et al., Adv. Electron. Mater. **4**, 1600501 (2018).
3) S. Chowdhury, B. L. Swenson, M. H. Wong, and U. K. Mishra, Semicond. Sci. Technol. **28**, 074014 (2013).
4) H. Fu, K. Fu, S. Chowdhury, T. Palacios, and Y. Zhao, IEEE Trans. Electron Devices **68**, 3200 (2021).
5) Y. Sun, X. Kang, Y. Zheng, J. Lu, X. Tian, K. Wei, H. Wu, W. Wang, X. Liu, and G. Zhang, Electronics **8**, 575 (2019).
6) I. C. Kizilyalli, A. P. Edwards, O. Aktas, T. Prunty, and D. Bour, IEEE Trans. Electron Devices **62**, 414 (2015).
7) K. Mukherjee et al., Materials **14**, 2316 (2021).
8) J. Hsu, M. Manfra, R. Molnar, B. Heying, and J. Speck, Appl. Phys. Lett. **81**, 79 (2002).
9) E. C. H. Kyle, S. W. Kaun, P. G. Burke, F. Wu, Y.-R. Wu, and J. S. Speck, J. Appl. Phys. **115**, 193702 (2014).
10) F. Kaess et al., J. Appl. Phys. **120**, 105701 (2016).
11) T. Narita et al., Jpn. J. Appl. Phys. **59**, SA0804 (2020).
12) H. Fujikura, T. Konno, T. Kimura, Y. Narita, and F. Horikiri, Appl. Phys. Lett. **117**, 012103 (2020).
13) N. Sawada, T. Narita, M. Kanechika, T. Uesugi, T. Kachi, M. Horita, T. Kimoto, and J. Suda, Appl. Phys. Express **11**, 041001 (2018).
14) Y. Zhang, Z. Chen, W. Li, A. R. Arehart, S. A. Ringel, and H. Zhao, Phys. Status Solidi A **218**, 2000469 (2021).
15) T. Tanaka, N. Kaneda, T. Mishima, Y. Kihara, T. Aoki, and K. Shiojima, Jpn. J. Appl. Phys. **54**, 041002 (2015).
16) M. Horita, T. Narita, T. Kachi, and J. Suda, Appl. Phys. Express **13**, 071007 (2020).
17) T. Narita, M. Horita, K. Tomita, T. Kachi, and J. Suda, Jpn. J. Appl. Phys. **59**, 105505 (2020).
18) Y. Zhang, Z. Chen, W. Li, H. Lee, M. R. Karim, A. R. Arehart, S. A. Ringel, S. Rajan, and H. Zhao, J. Appl. Phys. **127**, 215707 (2020).
19) T. Kimura, T. Konno, and H. Fujikura, Appl. Phys. Lett. **118**, 182104 (2021).
20) P. Reddy, S. Washiyama, F. Kaess, R. Kirste, S. Mita, R. Collazo, and Z. Sitar, J. Appl. Phys. **122**, 245702 (2017).
21) P. Reddy, F. Kaess, J. Tweedie, R. Kirste, S. Mita, R. Collazo, and Z. Sitar, Appl. Phys. Lett. **111**, 152101 (2017).
22) P. Reddy et al., J. Appl. Phys. **120**, 185704 (2016).
23) F. Kaess, P. Reddy, D. Alden, A. Klump, L. H. Hernandez-Balderrama, A. Franke, R. Kirste, A. Hoffmann, R. Collazo, and Z. Sitar, J. Appl. Phys. **120**, 235705 (2016).
24) D. C. Look and J. R. Sizelove, Appl. Phys. Lett. **79**, 1133 (2001).
25) K. Ueno, A. Kobayashi, and H. Fujioka, AIP Adv. **9**, 075123 (2019).
26) D. Huang et al., Solid State Electron. **45**, 711 (2001).
27) R. Y. Korotkov, J. M. Gregie, and B. W. Wessels, Appl. Phys. Lett. **80**, 1731 (2002).
28) J. Neugebauer and C. G. Van de Walle, Appl. Phys. Lett. **69**, 503 (1996).